Proc. Natl. Acad. Sci. USA
Vol. 92, pp. 860–864, January 1995
Cell Biology

Separation of human breast cancer cells from blood by differential dielectric affinity

FREDERICK F. BECKER*†, XIAO-BO WANG*, YING HUANG*, RONALD PETHIG‡, JODY VYKOUKAL*, AND PETER R. C. GASCOYNE*

*Department of Molecular Pathology, Box 89, University of Texas MD Anderson Cancer Center, 1515 Holcombe Boulevard, Houston, TX 77030; and ‡Institute of Molecular and Biomolecular Electronics, University of Wales, Dean Street, Bangor, Gwynedd LL57 1UT, United Kingdom

Communicated by Arthur B. Pardee, Dana–Farber Cancer Institute, Boston, MA, October 17, 1994

ABSTRACT **Electrorotation measurements were used to demonstrate that the dielectric properties of the metastatic human breast cancer cell line MDA231 were significantly different from those of erythrocytes and T lymphocytes. These dielectric differences were exploited to separate the cancer cells from normal blood cells by appropriately balancing the hydrodynamic and dielectrophoretic forces acting on the cells within a dielectric affinity column containing a microelectrode array. The operational criteria for successful particle separation in such a column are analyzed and our findings indicate that the dielectric affinity technique may prove useful in a wide variety of cell separation and characterization applications.**

Cell separation has numerous applications in medicine, biotechnology, and research and in environmental settings. For example, the use of autologous bone marrow transplants in the remediation of advanced cancers requires the removal of cancer cells from the patient's marrow (1), the study of signaling between blood cells requires purified cell subpopulations (2), and the purification of contaminated water supplies necessitates elimination of parasites such as *Giardia* and *Cryptosporidium* (3, 4). Current sorting technologies usually exploit differences in cell density, immunologic targets, or receptor–ligand interactions. These techniques are often inadequate, producing insufficiently pure cell populations, being too slow, or being too limited in the spectrum of target cells. Identification of novel properties by which different cell types may be discerned and of new ways for their selective manipulation are clearly fundamental components for improving sorting methodologies.

A particle suspended in a medium of different dielectric characteristics becomes electrically polarized when subjected to an alternating electrical field. Interaction between this induced polarization and the field gives rise to various electrokinetic effects. For example, a spatially inhomogeneous field will exert a lateral dielectrophoretic (DEP) force on the particle, directing it toward the minimum of dielectric potential (5–9), while a rotating field will induce particle electrorotation (ROT; refs. 10–12). The frequency dependencies of the magnitude and direction of these forces are functions of the intrinsic electrical properties of the particle that depend on the particle constitution and structural organization (13–15). For living cells, these characteristics are defined by composition, morphology, and phenotype (16, 17). Thus, DEP and ROT have been used to study bacteria (18), yeasts (11, 19), plant cells (10), and mammalian cells (20, 21) and to investigate cellular alterations accompanying physiological changes such as mitotic stimulation (16) and induced differentiation (7, 17, 21).

The publication costs of this article were defrayed in part by page charge payment. This article must therefore be hereby marked "*advertisement*" in accordance with 18 U.S.C. §1734 solely to indicate this fact.

Cells possessing dissimilar dielectric properties experience different DEP forces, suggesting two approaches by which cells might be separated—namely DEP migration and retention. In the first method, different cell types would be caused to experience forces in opposite directions by judicious choice of the applied field and suspending medium characteristics, as demonstrated on a microscopic scale (8, 22, 23). The second scheme would depend upon DEP entrapment of cells in potential energy wells whose depths depend on the cellular dielectric properties. By applying an appropriate external force, such as fluid flow, cells in shallow wells would be swept away and harvested while others would remain held in place by the DEP forces. Through such means DEP offers the potential not only to discriminate between but also to separate different cell types.

We show that the dielectric characteristics of cultured breast cancer cells are significantly different from those of blood cells. Next, we demonstrate how these differences can be exploited in a *dielectric affinity column* to remove tumor cells from dilute blood. Finally, we discuss the forces involved in dielectric separation and deduce the necessary conditions for it to occur.

MATERIALS AND METHODS

Cells. Peripheral blood was collected by venipuncture into 90 parts Ca^{2+}/Mg^{2+}-free phosphate-buffered saline containing 5 mM hemisodium EDTA to prevent clotting. T lymphocytes were obtained from (human immunodeficiency virus- and hepatitis-negative) Buffy bags (Gulf Coast Regional Blood Bank, Houston) following sheep erythrocyte rosetting (24). MDA231 cells, originally derived from a pleural effusion of a patient with metastatic breast cancer (25, 26), were cultured in minimum essential/F12 medium containing 10% fetal bovine serum, 1 mM glutamine, and 20 mM Hepes. They were harvested at ≈80% confluence 48 hr after seeding by a brief exposure to 0.25% trypsin/0.02% EDTA.

Dielectric Characterization. ROT measurements (10–12, 17, 19, 20) were made in which cells are subjected to a rotating electric field and thereby induced to rotate on an essentially stationary axis. They were reproducible and convenient because cells did not move to locations on the electrode array having different field strengths as they did in DEP experiments. Cells were diluted to a concentration of $\approx 5 \times 10^4$ per ml with (isotonic) 8.5% (wt/vol) sucrose plus 0.3% (wt/vol) dextrose buffer and adjusted with hemisodium EDTA to a suspension conductivity of 56 mS/m, to maximize the accuracy of derived dielectric parameters (27). Next, an aliquot of cell suspension was sealed into the electrode chamber and cells settled for 30 sec onto the glass substrate of a polynomial electrode (21, 28). ROT spectra were measured by timing rotation rates of individual cells located between the four

Abbreviations: DEP, dielectrophoretic; ROT, electrorotation.
†To whom reprint requests should be addressed.

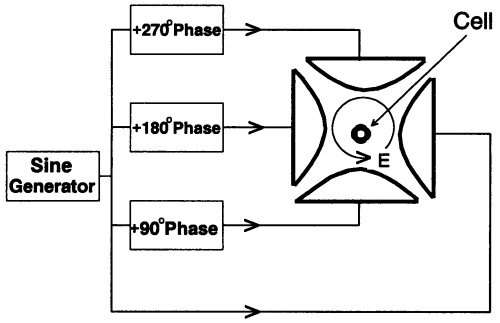

FIG. 1. ROT method for determining cellular dielectric properties using a thin gold polynomial electrode array of 400-μm tip–tip spacing. Cells were subjected to a rotating electrical field, E, generated by the application of sine signals in phase quadrature. Individual cell rotation rates were timed as a function of frequency with the aid of video microscopy.

electrode poles. A rotating field between 10 kHz and 100 MHz was established by applying sinusoidal waves (1 V rms) in phase quadrature to the electrode array (Fig. 1) from a custom-built signal generator (29).

Separation Procedure. The chamber was constructed of a glass plate spaced 60 μm above an array of interleaved gold electrodes on a glass substrate, fabricated using photolithography. The array covered an area of 17.6 mm × 55 mm and the electrode element width and spacing were 80 μm. Fluids were injected and removed through slots at each end of the chamber. The outlet was furnished with a well to trap cells exiting the chamber. Prior to experiments, the chamber was soaked for 5 min with 20% (wt/vol) bovine serum albumin solution to render the glass surfaces less adherent to cells. Alternate electrodes were connected to sinusoidal voltages of fixed or swept frequencies, monitored with an oscilloscope. Laminar flow of an eluate buffer was controlled by digital syringe pumps connected in push–pull configuration between inlet and outlet slots. A bubble-free fluid path was maintained at all times.

Mixtures of MDA231 breast cancer cells and blood were used to test the separation chamber. These were washed twice in isotonic 8.5% sucrose plus 0.3% dextrose, resuspended at a final concentration of 1×10^7 malignant cells and 3×10^7 normal blood cells per ml in this same medium, and adjusted to a conductivity of 10 mS/m with hemisodium EDTA. Following injection of $\approx$30 μl of cell mixture ($\approx 1.2 \times 10^6$ cells) to half fill the chamber, a 200-kHz signal of 5 V peak–peak was applied to the electrode array for 30 sec to collect all cells at the electrode tips by positive DEP. Flow of eluate (cell-free suspension buffer having a conductivity of 10 mS/m) was started at 5 μl/min and the applied frequency was lowered until blood cells were selectively released and trapped in the collection well (see *Results*). After 20 min, cells were removed from the well by cross-flow between two additional syringe ports. The voltage was then turned off to release the tumor cells held by DEP and these were eluted and collected separately. Slides were made of the two cell fractions to confirm their status as normal or malignant by Liu's modified Wright staining.

RESULTS

Cell Dielectric Responses. Fig. 2*A* shows typical ROT spectra for the cell lines investigated. Cells rotated counter to the field below 3, 5.5, and 7 MHz for MDA231 cells, lymphocytes, and erythrocytes, respectively; above these frequencies cofield rotation occurred. Counterfield rotation peaks occurred at 90, 400, and 550 kHz for these cells types, respectively. Differences in the dielectric characteristics were further

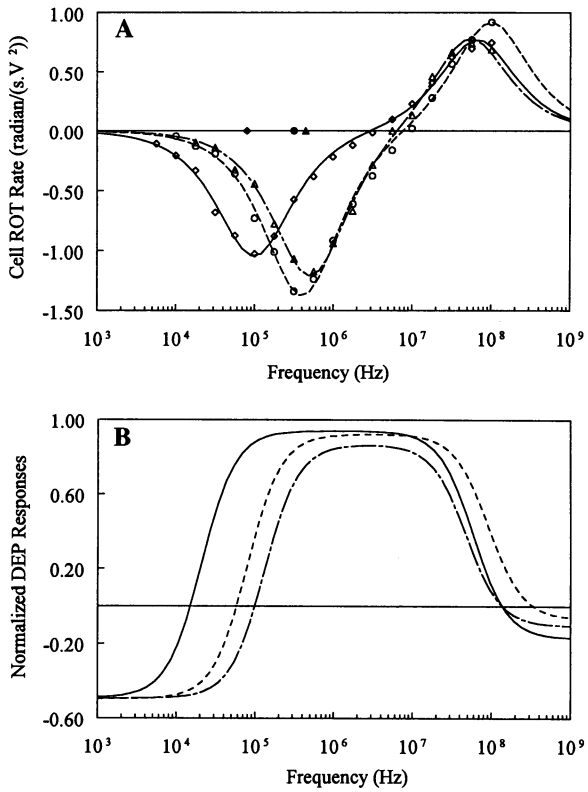

FIG. 2. (*A*) Typical ROT spectra for MDA231 cells (◇), T lymphocytes (○), and erythrocytes (△) in isotonic sucrose of conductivity 56 mS/m. Each point is the average of four stopwatch measurements. Statistical analysis showed the relative measurement error has a zero-mean and 0.05 variance. Continuous curves show best fits of the single-shell dielectric model (17, 19, 30). Measured DEP crossover frequencies are shown by the filled symbols. (*B*) DEP spectra for MDA231 cells (——), T lymphocytes (– – –), and erythrocytes (—·—) under separation conditions (conductivity 10 mS/m) calculated using the dielectric parameters derived from ROT measurements. Forces are normalized to equal effective polarizabilities (Eq. **1**).

examined by measurements of the DEP crossover frequency. At this frequency the direction of the DEP force changes, as frequency increases, from being directed away from, to being directed toward, the electrode tips. By switching the signals to the polynomial electrodes from ROT mode (signals in quadrature) to DEP mode (signals in opposition), the crossover frequencies were found to be 80, 320, and 450 kHz, respectively, for the three cell types.

These measurements demonstrated significant differences between the dielectric properties of MDA231 cells, erythrocytes, and T lymphocytes. To quantify these differences we optimized the parameters of the single-shell dielectric model (19, 20, 30) to fit the measured ROT spectrum for each cell as described previously (17). The derived parameters, with standard deviations, are given in Table 1. Using these dielectric parameters, we then applied the single shell model to calculate the expected frequency dependency of the DEP forces under our separation conditions. As shown in Fig. 2*B*, the DEP mean crossover frequencies were found to be 15, 58, and 95 kHz for MDA231, T lymphocytes, and erythrocytes, respectively, for a suspension conductivity of 10 mS/m. These DEP crossover frequency values enable us to select frequencies that best promote DEP separation.

Cell Separations. Following initial DEP collection of all cells (Fig. 3*A*), eluate flow was started at 5 μl/min and electrical signals were adjusted to meet two different aims: (*i*) *Maximal retention of tumor cells* was achieved by lowering the field frequency from 200 to 80 kHz. Blood cells were then

Table 1. Dielectric parameters for MDA231 cells, T lymphocytes, and erythrocytes

Cell type	$C_{specific}$, mF/m²	σ_{int}, S/m	ε_{int}
MDA231	26 ± 4.2	0.62 ± 0.073	52 ± 7.3
T lymphocytes	11 ± 1.1	0.76 ± 0.058	64 ± 5.9
Erythrocytes	9 ± 0.80	0.52 ± 0.051	57 ± 5.4

Specific membrane capacitance $C_{specific}$ and the internal conductivity σ_{int} and permittivity ε_{int} of the single-shell dielectric model were determined for individual cells from parameter optimization of ROT spectra over the frequency range 10 kHz to 100 MHz. The results are means ± standard deviations for 20 cells. Membrane conductance values derived from the analysis were so small that they did not contribute significantly to the measured ROT and DEP responses and could not be determined accurately (27).

released, eluted, and collected in the chamber outlet well. *All* tumor cells remained on the electrode tips under the DEP force and none could be detected in stained slides of the eluted fraction; typically, such slides contained ≈10,000 cells. Some blood cells were retained in the chamber due to entrapment within rafts of tumor cells; however, the ratio of blood cells to tumor cells fell to about 1:1. (*ii*) *Maximal purification of tumor cells* was accomplished (Fig. 3) by repetitively sweeping the applied field (twice per second) from 80 to 20 kHz during cell release. This shook loose entrapped blood cells by reducing the packing density of the collected cells. Blood cells then became levitated from electrode surfaces and were eluted.

The sequence of cell separation is shown in Fig. 3. After collection at 200 kHz (Fig. 3*A*) the swept signal was applied.

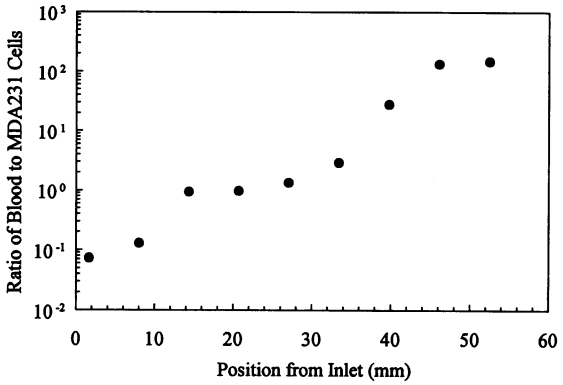

FIG. 4. Cell distribution on the dielectric affinity electrode array as a function of distance from the inlet 12 min after cell sorting was commenced (see text).

Blood cells became focused into bands that flowed between the electrode tips (Fig. 3*B*), leaving the cancer cells behind (Fig. 3*C*). Toward the chamber outlet, only blood cells moved in focused bands (Fig. 3*D*). Twelve minutes after application of the swept signal, the cell distribution on the electrodes was examined (Fig. 4). With increasing distance from the inlet, the ratio of erythrocytes to MDA231 cells increased from 1:15 to 1:1 and remained at that value where the chamber had been initially loaded with cells. Thereafter, the proportion of erythrocytes rapidly increased, reaching in excess of 99% at the outlet. After 20 min, retained tumor cell fractions were >95% pure.

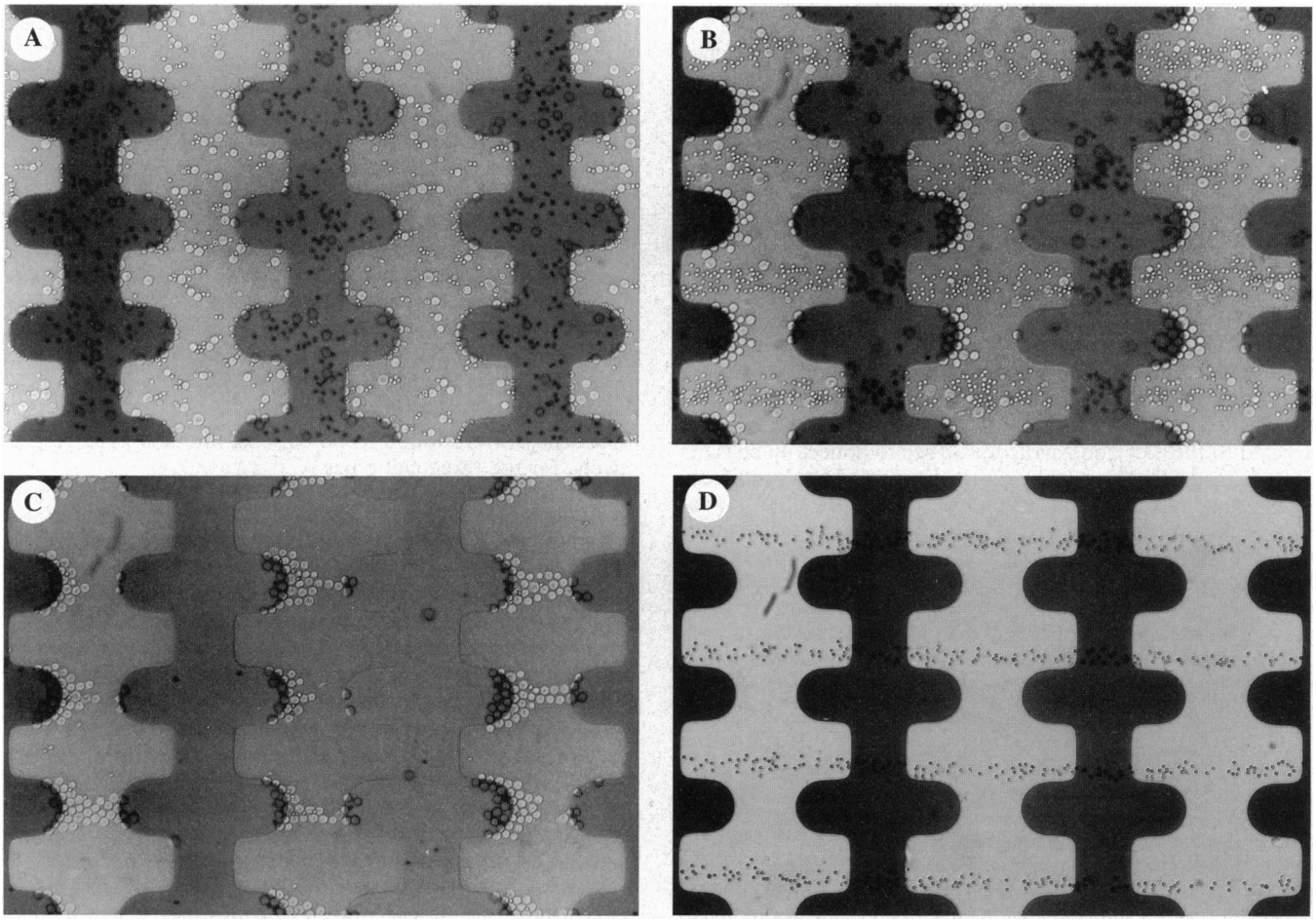

FIG. 3. Separation of MDA231 human metastatic breast cancer (larger cells) from dilute peripheral blood (see text). (*A*) During initial collection. (*B*) During release (fluid flow from left to right). (*C*) Cancer cells remained on the electrode tips after blood cells had been swept downstream. (*D*) Close to the outlet, where the chamber had not initially been loaded with cells, only blood cells, in focused bands, were moving.

The swept-frequency protocol resulted in the escape of some tumor cells with eluted blood cells. Nevertheless, stained slides of the eluted fractions still revealed a 58-fold reduction in the concentration of tumor cells.

Cell Viability Following Sorting. Greater than 98% of cells excluded trypan blue dye following sorting, indicating that membrane barrier function was maintained. We also assessed the effect of DEP collection on growth of cancer cells. MDA231 cells (10^6) were collected for 10 min at electrode tips at 300 kHz and flushed into a T-25 tissue culture flask containing complete medium. A control sample was seeded in parallel. At 48 hr when the control reached confluence, the DEP-collected sample had reached 80% confluence, suggesting a minimal loss of viability, or lag in the reestablishment of growth, occurred in DEP-collected cells. Since normal cells in separation experiments were subjected to less field exposure than tumor cells, it is reasonable to assume that they, too, were viable.

DISCUSSION

Dielectric Properties of Cells. Cell DEP and ROT behaviors have been interpreted in terms of increasing penetration of the applied electrical field through the plasma membrane with increasing frequency (11, 17, 31, 32). Thus, DEP and ROT responses below 1 MHz are dominated by dielectric properties of the plasma membrane. As shown in Fig. 2, significant differences exist between the electrokinetic behaviors of MDA231, lymphocytes, and erythrocytes in this frequency range, indicating that the membrane dielectric properties differ between these cells. This is confirmed by the derived membrane-specific capacitances (Table 1).

Specific capacitance of the plasma membrane reflects membrane morphological features, including microvilli, membrane folds, and blebbing (12, 16, 17). Thus, the large differences between MDA231 cells, lymphocytes, and erythrocytes found here almost certainly arise from membrane morphological differences. Because separation depended upon dielectric differences between cell types at low frequencies, it exploited such cell surface physical characteristics as a sorting criterion.

Cell viability was not seriously affected by DEP sorting, as judged by trypan blue and cell growth experiments. This is not surprising since cells have been reported to remain viable even following electrical manipulations such as electroporation and electrofusion that typically operate at induced pulsed membrane potentials in excess of 0.5 V (33, 34). Our field strengths induced sinusoidal membrane potentials of <0.2 V.

Separation Mechanics. Our technique balances hydrodynamic forces from a laminar-flow profile against DEP forces. Cells experienced forces from gravity, dielectrophoresis, fluid drag, and hydrodynamic lift effects (Fig. 5). The DEP force acting on a cell of radius r is given by (6–9)

$$\vec{F}_{\mathrm{DEP}} = 4\pi r^3 \varepsilon_{\mathrm{m}} \alpha V^2 (k_{\mathrm{x}} \vec{a}_{\mathrm{x}} + k_{\mathrm{y}} \vec{a}_{\mathrm{y}}), \qquad [1]$$

where ε_{m} = dielectric permittivity of the eluate; V = peak–peak electrode voltage, and α is the real part of the Clausius–Mossotti factor (6–9) expressing the effective polarizability of the cell in the eluate. Depending on the polarity of α, the DEP force directs cells toward either strong or weak field regions. k_{x} and k_{y} are the maximum vertical and horizontal components, respectively, of the field nonuniformity factor $\nabla E^2_{\mathrm{rms}}$ (5–9) for an applied 1-V peak–peak voltage. These depend on the electrode geometry and become larger when a cell is closer to an electrode tip (8, 21, 22).

The horizontal drag due to fluid motion on a cell in contact with a wall is given (35) by

$$F_{\mathrm{HORIZ}} \cong 6\pi c r \eta (v_{\mathrm{m}} - v_{\mathrm{p}}), \qquad [2]$$

where η = dynamic viscosity of the eluate, v_{p} = cell velocity, c = 1.7. v_{m} is the fluid velocity at the cell center and follows a parabolic profile

$$v_{\mathrm{m}} = 6\langle v \rangle \frac{x}{w}\left(1 - \frac{x}{w}\right), \qquad [3]$$

where $\langle v \rangle$ = mean velocity of eluate, w = top to bottom wall spacing, and x = distance from the chamber bottom. The lift force experienced by a cell a small distance $x - r$ above the chamber wall (36) is given by

$$F_{\mathrm{LIFT}} \cong 0.153 r^3 \eta \frac{1}{(x-r)} \cdot \left.\frac{dv_{\mathrm{m}}}{dx}\right|_{x=0}. \qquad [4]$$

The nature of this force remains in question although detailed theoretical analyses of inertial lift effects and shear-induced diffusion have been given (36–38).

The separation chamber operated under conditions where the maximum DEP force F_{DEP} for one cell type (radius r_1) prevailed against the horizontal drag F_{HORIZ} and the hydrodynamic lift F_{LIFT}, causing this cell type to be retained on the electrode tips while others (radius r_2) were eluted. Thus, the chamber had selective dielectric affinity for one cell type. Combining Eqs. **1–3**, we derive the condition for separation to occur:

$$r_1 \alpha_1 k_{\mathrm{y1}} > \beta \frac{\langle v \rangle}{V^2} > r_2 \alpha_2 k_{\mathrm{y2}}, \qquad [5]$$

where $\beta = 36\pi c\eta / w\varepsilon_{\mathrm{m}}$ is a constant for a given chamber and eluate. The left- and right-hand terms define the properties of the different cell types, while the center term reflects the competition between the fluid flow rate $\langle v \rangle$ and the DEP forces due to the applied voltage V. Eq. **5** assumes cells were initially stationary at the chamber bottom. Good separation can be obtained if the product of the cell radii and dielectric polarizabilities are sufficiently different and the ratio of fluid velocity to the square of the applied voltage is within the specified range.

To compare Eq. **5** with our observations, we used the charge density method (8) to calculate the field distribution for our electrode using a FORTRAN program running on a Cray YMP computer; k_{y} was found to have the value 1.8×10^{12} per m^3. For our mean flow rate of 95 μm/sec and applied peak–peak voltage of 5 V, Eq. **5** predicts that cells of radius 5 μm and a polarizability in excess of 0.27 should be dielectrophoretically retained, while cells of smaller polarizability or radius should be eluted. Fig. 2*B* shows that MDA231 cells and erythrocytes had mean polarizabilities at 80 kHz of 0.7 and −0.1, respectively. Combining these values with k_{y}, we found the DEP force on MDA231 cells was strongly attractive and exceeded F_{HORIZ}

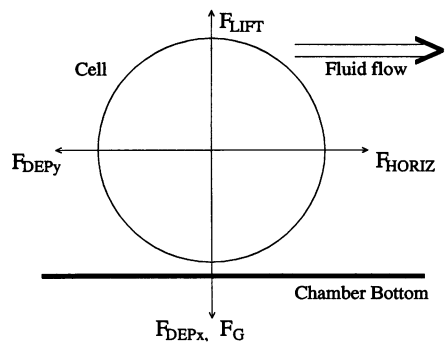

FIG. 5. Forces affecting cells within the dielectric affinity column: gravity (F_{G}), dielectrophoresis (F_{DEPx}, F_{DEPy}), fluid drag (F_{HORIZ}), and hydrodynamic lift effects (F_{LIFT}).

by a factor of 4, accounting for their collection. By contrast, the force on erythrocytes was repulsive, explaining why they were focused into bands that flowed in the low-field regions of the electrode array.

The swept-frequency protocol was designed to release blood cells entrapped within masses of tumor cells by obstruction and DEP cell–cell interactions (39). By lowering the frequency to 20 kHz, just above the mean crossover frequency for MDA231 cells, the packing of cells at the electrode tips and the strength of cell–cell interactions were lessened. Furthermore, the repulsive DEP force on blood cells was increased. The combined effect was to facilitate the release of erythrocytes. Collected MDA231 cells could have become dislodged under these conditions, and sweeps back to 80 kHz repacked them and minimized their probability of release.

Our technique has some similarities to field-flow fractionation in which F_G and F_{LIFT} are balanced and particles equilibrate at characteristic positions within a flow profile and elute at different rates. However, it differs in that the DEP force is sufficient to immobilize particles and retain them indefinitely, providing for almost perfect separation. Our method not only utilizes differences in particle sizes and densities as sorting criteria but also, and more importantly, exploits their differential dielectric properties. A hybrid technology of dielectric affinity and field-flow fractionation may be applicable to a wide variety of separation problems.

Our prototype column sorted cells at a rate of about 10^3 per sec; larger devices could increase this rate by 2 orders of magnitude, much faster than fluorescent-activated and other refined sorters. Furthermore, our technique is noninvasive and does not depend on antibodies or cell surface antigens, making it attractive for separating leukocyte subpopulations without possible problems of cell activation.

Finally, differential DEP migration has been used to separate viable from nonviable yeast (8, 40), erythrocytes from bacteria (8), erythrocytes from erythroleukemia cells (22), and Gram-positive from Gram-negative bacteria (23) over distances of the order 100 μm. We believe, therefore, that the technique of differential dielectric affinity described here has important implications for a wide range of separation problems and represents a powerful tool for discriminating between cell populations of fundamental research and clinical interest.

We thank Prof. Garth Nicolson and Dr. Philip Cavanaugh for MDA231 cells, Jamileh Noshari and Linda Yoshimura for cell preparation, and John Tame for photolithography. This work was supported by the Texas Higher Education Coordinating Board Advanced Technology Program and the Sid W. Richardson Foundation.

1. Fischer, A. (1993) *Br. J. Haematol.* **83,** 531–534.
2. Hathcock, K. S., Hirano, H. & Hodes, R. J. (1993) *Immunol. Res.* **12,** 21–36.
3. Crawford, F. G. & Vermund, S. H. (1988) *CRC Crit. Rev. Microbiol.* **16,** 113–159.
4. Rose, J. B., Landeen, L. K., Riley, K. R. & Gerba, C. P. (1989) *Appl. Environ. Microbiol.* **55,** 3189–3196.
5. Pohl, H. A. (1978) *Dielectrophoresis* (Cambridge Univ. Press, Cambridge, U.K.).
6. Hölzel, R., Lamprecht, I. & Mischel, M. (1991) in *Physical Characterization of Biological Cells*, eds. Schütt, W., Klinkmann, H., Lamprecht, I. & Wilson, T. (Gesundheit, Berlin), pp. 273–294.
7. Gascoyne, P. R. C., Pethig, R., Burt, J. P. H. & Becker, F. F. (1993) *Biochim. Biophys. Acta* **1149,** 119–126.
8. Wang, X.-B., Huang, Y., Burt, J. P. H., Markx, G. H. & Pethig, R. (1993) *J. Phys. D Appl. Phys.* **26,** 1278–1285.
9. Kaler, K. V. I. S. & Jones, T. B. (1990) *Biophys. J.* **57,** 173–182.
10. Fuhr, G., Rosch, P., Müller, T., Dressler, V. & Goring, H. (1990) *Plant Cell Physiol.* **31,** 975–985.
11. Hölzel, R. & Lamprecht, I. (1992) *Biochim. Biophys. Acta* **1104,** 195–200.
12. Sukhorukov, V. L., Arnold, W. M. & Zimmermann, U. (1993) *J. Membr. Biol.* **132,** 27–40.
13. Grant, E. H., Sheppard, R. J. & South, G. P. (1978) *Dielectric Behaviour of Biological Molecules in Solution* (Clarendon, Oxford).
14. Pethig, R. & Kell, D. B. (1987) *Phys. Med. Biol.* **32,** 933–970.
15. Pethig, R. (1979) *Dielectric and Electronic Properties of Biological Materials* (Wiley, Chichester, U.K.).
16. Hu, X., Arnold, W. M. & Zimmermann, U. (1990) *Biochim. Biophys. Acta* **1021,** 191–200.
17. Wang, X.-B., Huang, Y., Gascoyne, P. R. C., Becker, F. F., Hölzel, R. & Pethig, R. (1994) *Biochim. Biophys. Acta* **1193,** 330–344.
18. Price, J. A. R., Burt, J. P. H. & Pethig, R. (1988) *Biochim. Biophys. Acta* **964,** 221–230.
19. Huang, Y., Hölzel, R., Pethig, R. & Wang, X.-B. (1993) *Phys. Med. Biol.* **37,** 1499–1517.
20. Gimsa, J., Marszalek, P., Loewe, U. & Tsong, T. Y. (1991) *Biophys. J.* **60,** 749–760.
21. Gascoyne, P. R. C., Noshari, J., Becker, F. F. & Pethig, R. (1994) *IEEE Trans. Ind. Appl.* **30,** 829–834.
22. Gascoyne, P. R. C., Huang, Y., Pethig, R., Vykoukal, J. & Becker, F. F. (1992) *Meas. Sci. Technol.* **3,** 439–445.
23. Markx, G. H., Huang, Y., Zhou, X.-F. & Pethig, R. (1994) *Microbiology* **140,** 585–591.
24. Jondal, M., Holm, G. & Wigzell, H. (1972) *J. Exp. Med.* **136,** 207–215.
25. Cailleau, R., Olive, M. & Cruciger, Q. V. J. (1978) *In Vitro* **14,** 911–915.
26. Zhang, R. D., Fidler, I. J. & Price, J. E. (1991) *Invasion Metastasis* **11,** 204–215.
27. Gascoyne, P. R. C., Wang, X.-B. & Becker, F. F. (1994) *Bioelectrochem. Bioenerg.*, in press.
28. Huang, Y. & Pethig, R. (1991) *Meas. Sci. Technol.* **2,** 1142–1146.
29. Hölzel, R. (1993) *IEEE Trans. Instrum. Meas.* **42,** 758–760.
30. Irimajiri, A., Hanai, T. & Inouye, A. (1979) *J. Theor. Biol.* **78,** 251–269.
31. Glaser, R. & Fuhr, G. (1987) in *Mechanistic Approaches to Interactions of Electric and Electromagnetic Fields With Living Matter*, eds. Blank, M. & Findl, E. (Plenum, New York), pp. 271–290.
32. Arnold, W. M. & Zimmermann, U. (1988) *J. Electrostat.* **21,** 151–191.
33. Sugar, I. P. & Neumann, E. (1984) *Biophys. Chem.* **19,** 211–225.
34. Wolf, H., Rols, W. P., Boldt, E., Neumann, E. & Teissié, J. (1994) *Biophys. J.* **66,** 524–531.
35. O'Neill, M. E. (1968) *Chem. Eng. Sci.* **23,** 1293–1298.
36. Williams, P. S., Koch, T. & Giddings, J. C. (1992) *Chem. Eng. Commun.* **111,** 121–147.
37. Leighton, D. & Acrivos, A. (1985) *J. Appl. Math. Phys.* **36,** 174–178.
38. Leighton, D. & Acrivos, A. (1987) *J. Fluid Mech.* **181,** 415–439.
39. Mehrle, W., Hampp, R., Zimmermann, U. & Schwan, H. P. (1988) *Biochim. Biophys. Acta* **939,** 561–568.
40. Markx, G. H., Talary, M. & Pethig, R. (1994) *J. Biotechnol.* **32,** 29–37.